Shear effects on passive scalar spectra

By A. C E L A N I[1,2], M. C E N C I N I[3], M. V E R G A S S O L A[4], E. V I L L E R M A U X[5] AND D. V I N C E N Z I[2,6]

[1]CNRS, INLN, 1361 Route des Lucioles, F-06560 Valbonne, France

[2]CNRS UMR 6202, Observatoire de la Côte d'Azur, B.P. 4229, 06304 Nice Cedex 4, France

[3]Center for Statistical Mechanics and Complexity, INFM Roma 1 and Dipartimento di Fisica, Università di Roma "La Sapienza", Piazzale Aldo Moro, 2, I-00185 Roma, Italy

[4]CNRS, URA 2171, Institut Pasteur, 28, rue du Dr. Roux, 75724 Paris Cedex 15, France

[5]Univ. Aix Marseille 1, IRPHE, 49, rue Frederic Joliot Curie, F-13384 Marseille 13, France

[6]Dép. de Mathématiques, Univ. de Nice-Sophia Antipolis, Parc Valrose, 06108 Nice, France

The effects of a large-scale shear on the energy spectrum of a passively advected scalar field are investigated. The shear is superimposed on a turbulent isotropic flow, yielding an Obukhov–Corrsin $k^{-5/3}$ scalar spectrum at small scales. Shear effects appear at large scales, where a different, anisotropic behaviour is observed. The scalar spectrum is shown to behave as $k^{-4/3}$ for a shear fixed in intensity and direction. For other types of shear characteristics, the slope is generally intermediate between the $-5/3$ Obukhov–Corrsin and the -1 Batchelor values. The physical mechanisms at the origin of this behaviour are illustrated in terms of the motion of Lagrangian particles. They provide an explanation for the scalar spectra that are shallow and dependent on the experimental conditions in shear flows at moderate Reynolds numbers.

1. Introduction

Two major regimes are known for a passive scalar field transported by a turbulent flow. The first, known as inertial–convective, refers to the range of scales where the direct effects of the fluid viscosity and the scalar diffusivity are both negligible. The predicted behaviour of the spectrum $E_\theta(k)$ of the scalar field θ is (Obukhov 1949; Corrsin 1951):

$$E_\theta(k) = C\epsilon^{-1/3}\epsilon_\theta k^{-5/3}. \tag{1.1}$$

Here, k denotes the wavenumber, C is a non-dimensional constant, and ϵ and ϵ_θ are the average dissipation rates of the kinetic energy and the scalar variance, respectively. The second regime, dubbed viscous–convective, is at scales smaller than the first and holds for weakly diffusive (alternatively high Schmidt or Prandtl number) scalars. The velocity field is now smoothed out by the molecular viscosity, linearizing the dependence of the velocity increments on the separation between the two points where the increment is taken. This yields the Batchelor behaviour (Batchelor 1959):

$$E_\theta(k) \propto k^{-1}. \tag{1.2}$$

Scalar spectra have been measured in a number of laboratory experiments. None of these pure power laws with the exponents anticipated above are routinely observed. The existence of a k^{-1} spectrum in the viscous–convective subrange has been questioned based on high Reynolds and Schmidt number experiments (Miller & Dimotakis 1996; Warhaft 2000; Yeung, Xu & Sreenivasan 2002). At larger scales,

scalar spectra do behave compatibly with a power law, but their slope is often found to deviate from the Obukhov–Corrsin $-5/3$ value. Deviations are particularly important in turbulent shear flows, where the observations indicate that the spectra strongly depend on the Reynolds number Re (Mestayer 1982; Sreenivasan 1991, 1996; Miller & Dimotakis 1996; Warhaft 2000) and on the detailed set-up of the advecting turbulent flow. The prediction (1.1) is, in particular, recovered for very large Reynolds numbers only ($Re_\lambda > 2000$). Deviations are also observed when the velocity field displays a convincing $k^{-5/3}$ spectrum (see, e.g., Sreenivasan 1996; Villermaux, Innocenti & Duplat 2001).

Our aim here is to investigate the physical origin of the behaviour experimentally observed in shear flows, briefly recalled in §2. We specifically consider a model where the velocity is decomposed into a linear shear, superimposed onto a turbulent flow assumed to obey Kolmogorov's scaling. As in thermal convection and Navier–Stokes turbulence (see e.g. Siggia 1994; Casciola 2002), the presence of the shear introduces a new length scale r_c. The scalar spectrum crosses from the classical behaviour (1.1) at scales $r \ll r_c$ to a different anisotropic behaviour for $r \gg r_c$. As discussed in §3, Lagrangian dimensional arguments allow the scaling of the scalar spectrum in the new shear-regime to be predicted for a variety of shear properties. A $-4/3$ scaling is, in particular, found for a shear fixed in intensity and direction. A test of the Lagrangian dimensional arguments is provided in §4, where we consider a simpler turbulent flow with a short correlation time. The assumption is unphysical and the Lagrangian arguments of §3 yield quantitatively different predictions; the point is however that these predictions can be stringently tested against the exact solution for the scalar spectrum which can be obtained in this special case. The final Section is devoted to discussions and conclusions. The Appendix contains technical material used in §4.

2. Scalar spectra in experiments

Turbulent flows can be divided into two broad categories: shear flows (jets, wakes, and boundary layers) and flows where the effects of large-scale shears are tamed (e.g. grid-generated turbulence). The latter are the laboratory flows providing the closest physical realization of the homogeneous and isotropic turbulence dealt with by most theoretical fluid dynamics.

Various possible ways to inject scalar fields in turbulent flows have been employed. In grid turbulence, temperature fluctuations are generated by heating either the grid itself or small wires located thereafter. In shear flows, one possibility is to weakly heat the jet or the wall of the boundary layer. Alternatively, a colorant dye can be injected past the flow source, at a scale possibly different from that of the stirring source. Temperature time series are taken by a thermometer in a fixed location and, as customary in most fluid dynamics experiments, time intervals are converted to space distances by the Taylor hypothesis. Scalar spectra or, equivalently, second-order structure functions, are thus measured. The use of fluorescent dyes offers the possibility to extract cuts – usually two-dimensional – of the scalar field from the intensity field. Simultaneous velocity measurements are usually taken by anemometers. The reader interested in a detailed discussion of the experimental techniques is referred to Sreenivasan (1996), Warhaft (2000), Villermaux *et al.* (2001).

The observations collected in the literature might be summarized as follows. In grid-generated turbulence, the prediction (1.1) is well-verified. This also holds at moderate Re_λ, when there is a tiny range of scales where the spectrum of the velocity field displays a clean $-5/3$ slope. Some results obtained by directly heating the grid used to generate the turbulence have been criticised (Warhaft 2000) on account of

possible correlations between the temperature and the velocity. It seems, nevertheless, a well-established fact (see Jayesh, Tong & Warhaft 1994; Mydlarski & Warhaft 1998; Warhaft 2000) that the slope of the scalar spectrum increases with Re_λ from values $\simeq$ -1.5 to $-5/3$, reached at Reynolds numbers $Re_\lambda \geqslant 200$. Small deviations observed at lower Re_λ are confidently ascribed to finite-Re effects.

The situation in turbulent shear flows is more intricate. Experiments with different Re_λ but similar non-dimensional shear rates have been collected and compared by Sreenivasan (1996). The main observation is that the slopes of the passive scalar spectra display a strong dependence on the turbulent intensity. Their slope is approximately 1.3 at low Re_λ and attains the predicted $-5/3$ value at $Re_\lambda \geqslant 2000$ only. Strong anisotropic effects are also observed for the velocity energy spectrum. Indeed, its longitudinal component reaches the expected $-5/3$ behaviour at moderate $Re_\lambda (\approx 50)$. Conversely, its transverse component behaves more like the scalar field, with a slope continuously increasing with Re_λ and saturating to $-5/3$ only for $Re_\lambda \geqslant 3000$. The experiments by Villermaux *et al.* (2001) report even more severe deviations from (1.1), with a slope close to the Batchelor unit value, in spite of the $-5/3$ spectrum observed for the velocity field. The scalar injection scale, although still lying in the inertial range of scales, was smaller than the turbulence forcing scale in that case.

3. Shear effects on Lagrangian dynamics

The experimental observations presented in §2 naturally lead to the surmise that the deviations observed in the scalar spectra have, among other possibles causes, their origin in the presence of a sustained large-scale shear. The interplay between diffusion and shear is a classical problem first examined by Levèque (1928) for heat transport across boundary layers. Qualitatively, the flow stretches the distances between particles along the shear and sharpens the scalar gradient perpendicular to it, therefore altering the usual diffusion law.

In order to quantitatively assess the impact of shear on scalar spectra, we introduce the following simple model for the velocity field $v(r, t)$:

$$v(r, t) = \sigma y \,\hat{x} + u(r, t). \tag{3.1}$$

The flow is thus the superposition of an average linear shear of intensity σ directed along the x-direction and a turbulent fluctuating field u, assumed to obey Kolmogorov's scaling, for the sake of simplicity. The spectrum of the velocity field obeys, in particular, the classical $k^{-5/3}$ law.

A passive scalar field, $\theta(r, t)$, transported by the above flow is governed by the standard advection–diffusion equation:

$$\partial_t \theta + \sigma y \partial_x \theta + u \cdot \nabla \theta = \kappa \Delta \theta + f, \tag{3.2}$$

where κ is the molecular diffusivity and f is an external source of scalar fluctuations. The source is needed to maintain the system in a statistically steady state and we shall suppose that the forcing has a characteristic length L_f.

The transport equation (3.2) is equivalently recast in terms of the Lagrangian trajectories $\rho(t)$ of tracer particles. They obey the stochastic differential equation

$$d\rho = v(\rho, t)\,dt + \sqrt{2\kappa}\,dW, \tag{3.3}$$

where W is an isotropic Brownian motion and v is given by (3.1). The equation for the scalar field along the trajectories is the ordinary differential equation $d\theta/dt = f$, easily integrated. The scalar second-order correlation function of the scalar field is

then expressed as (see, e.g., Falkovich, Gawędzki & Vergassola 2001):

$$C_2(\boldsymbol{r}, t) = \langle \theta(\boldsymbol{r}, t)\theta(\boldsymbol{0}, t)\rangle = \int_{-\infty}^{t} \mathrm{d}s \int \mathrm{d}\boldsymbol{R}\, p(\boldsymbol{R}, s|\boldsymbol{r}, t)\,\chi(\boldsymbol{R}). \tag{3.4}$$

Here, $\boldsymbol{R}$ is the separation between two tracer particles and $p(\boldsymbol{R}, s|\boldsymbol{r}, t)$ is the propagator, i.e. the probability, averaged over the realizations of the velocity ensemble and of the Brownian noise, that a pair of particles is found separated by $\boldsymbol{R}$ at time s, conditional on its separation $\boldsymbol{r}$ at time t. The function $\chi(\boldsymbol{R})$ having its support at scales $R \leqslant L_f$, the integral (3.4) is roughly equal to $\chi(0)T(r, L_f)$, where $T(r, L_f)$ is the residence time at distances $\leqslant L_f$ for a pair of particles initially separated by a distance r. Analogously, the second-order structure function $S_2(r) = 2[C_2(0) - C_2(r)] \propto T(0, L_f) - T(r, L_f)$. The incompressibility of the flow ensures that the scaling of the latter quantity can be estimated as the time for two particles, initially coinciding, to reach a separation r.

The problem of determining the scaling behaviour of scalar spectra is thus reduced to the study of the evolution of the separation between a pair of particles.

For the case without shear, $\sigma = 0$, classical dimensional arguments give the Richardson law: $\langle R^2(t)\rangle \sim t^3$, which translates into a 2/3 scaling exponent for $S_2(r)$ and the ensuing Obukhov–Corrsin $-5/3$ slope for the scalar spectrum.

Let us now consider the case with shear, $\sigma \neq 0$. The components of the separation between two fluid particles obey the equations of motion:

$$\dot{R}_x = \sigma R_y + \delta u_x(\boldsymbol{R}, t), \tag{3.5}$$

$$\dot{\boldsymbol{R}}_\perp = \delta \boldsymbol{u}_\perp(\boldsymbol{R}, t), \tag{3.6}$$

where the dot indicates the time-derivative, $\delta \boldsymbol{u}$ is the velocity difference between the two particles and $\dot{\boldsymbol{R}}_\perp$ indicates the components of the velocity orthogonal to the shear. At small enough times, the turbulent component, which scales with exponent 1/3, dominates over the linear shear and Richardson's behaviour holds. The crossover to a different anisotropic behaviour occurs at $r_c \simeq \sigma^{-3/2}$. Those are the separations at which the shear and the turbulent components become comparable. The time required for two particles initially coinciding to reach those scales behaves as $t_c \propto \sigma^{-1}$. For $t \gg t_c$, the form of the Lagrangian equations naturally suggests that the parallel and the transverse components scale differently with time:

$$\langle R_x^2\rangle \approx \langle R^2\rangle \propto t^{2\alpha}, \qquad \langle R_\perp^2\rangle \sim t^{2\beta}. \tag{3.7}$$

Inserting this ansatz into (3.5) and (3.6), neglecting the δu_x term in (3.5) and using the Kolmogorov scaling $\delta \boldsymbol{u}_\perp(\boldsymbol{R}, t) \propto R^{1/3} \simeq t^{\alpha/3}$, we obtain the relations $\alpha - 1 = \beta$ and $\beta - 1 = \alpha/3$. We thus end up with the predictions $\alpha = 3$, $\beta = 2$ for the Lagrangian separations, which give

$$C_2(r) \propto r^{1/3}, \qquad E(k) \propto k^{-4/3}, \tag{3.8}$$

for the correlations of the scalar field, by using the arguments following (3.4).

It is worth emphasizing that the scalar statistics is sensitive to the shear characteristics, as expected for any passive transport. For example, if the direction of the shear were to rotate rapidly, isotropy would be recovered and the stretching of the separations among the particles would be dominated by the linear shear component, leading to an exponential-in-time separation and a k^{-1} behaviour. The physics is the same as in the Batchelor regime, but the behaviour now holds at large scales. The rapidity of the rotation should be gauged with respect to the Lagrangian turnover time: if τ_ϕ denotes the typical time of rotation, the fixed limit (3.1) holds for scales $r \ll \tau_\phi^{3/2}$ and the rapidly rotating asymptotics in the opposite limit. For

the fluctuations of the shear intensity, let us similarly denote by τ_σ its correlation time. The intensity is effectively fixed in time, as in (3.1), for scales $r \ll \tau_\sigma^{3/2}$. In the opposite limit, the intensity might be taken as a random process with a short correlation time $\langle \sigma(t)\sigma(t') \rangle = \sigma^2 \delta(t - t')$. Inserting the ansatz (3.7) into (3.5) leads now to the relation $\alpha - 1 = -1/2 + \beta$, giving a slope $-13/9$ for the scalar spectrum. The geometry of the shear and the ratio between its timescale and the turbulent turnover times are thus seen to affect the properties of a passively transported field. The point of interest in interpreting the experimental data is that the exponents of the spectra are in all cases smaller than $-5/3$, implying that the presence of a shear generally induces a crossover to a shallower spectrum at the large scales.

4. A solvable case

The aim of this Section is to test the dimensional arguments presented in the previous Section by investigating the simpler case of a turbulent flow $\boldsymbol{u}$ belonging to the Kraichnan ensemble (Kraichnan 1968). The rationale is as follows. The short correlation time of the velocity is unphysical and the Lagrangian predictions (3.8) are thereby modified (the scaling $-4/3$ of the scalar spectrum becoming, for example, $-11/9$). Yet, the point is that one can compare those predictions to the solution of the exact equation for the scalar spectrum. The advantage over a direct numerical simulation of the more realistic flows in §3 is that the range of scales available here is much more extended and the comparison is therefore quantitatively more stringent, albeit less direct.

The field $\boldsymbol{u}$ in (3.1) is taken now as an incompressible, statistically isotropic and homogeneous Gaussian field of zero mean and correlation function:

$$\langle [u_i(\boldsymbol{r}, t) - u_i(\boldsymbol{0}, t)][u_j(\boldsymbol{r}, 0) - u_j(\boldsymbol{0}, 0)] \rangle = \delta(t) \left\{ D\, r^\xi \left[(1 + \xi)\delta_{ij} - \xi \frac{r_i r_j}{r^2} \right] \right\}. \quad (4.1)$$

Here, we specialize to the two-dimensional case for the sake of simplicity: this choice has no qualitative consequences on the results. The parameter D measures the turbulent intensity and the velocity field is assumed to be scale-invariant with roughness exponent $\xi \in [0, 2]$. The presence of an ultraviolet viscous cutoff mimicking the Kolmogorov scale could be considered, but it will not be needed here.

Using standard methods of Gaussian integration by parts (see Falkovich *et al.* 2001), we can adapt the Lagrangian arguments of the previous section to the case of a Kraichnan flow. The Lagrangian separation law for the isotropic case is $\langle R^2(t) \rangle \propto t^{2/(2-\xi)}$. Note that the Richardson scaling is obtained for $\xi = 4/3$, differing from the $2/3$ of real turbulent flows due to the δ-correlation in time of the velocity field. For the anisotropic case of a shear fixed in intensity and direction, the relations between the exponents α and β stemming from (3.5) and (3.6) are now $\alpha - 1 = \beta$ and $2\beta - 1 = 2\alpha\xi$. Solving these relations gives the following behaviours of the Lagrangian separations and the scalar spectra:

$$\langle R_x^2 \rangle \approx \langle R^2 \rangle \propto t^{6/(2-\xi)}, \quad \langle R_y^2 \rangle \sim t^{2(1+\xi)/(2-\xi)}, \quad E(k) \propto k^{-(5-\xi)/3}. \quad (4.2)$$

For $\xi = 4/3$, (4.2) gives a $-11/9$ exponent for the scaling of the scalar spectrum.

The advantage of Kraichnan's flows is that the behaviour of the second-order correlation function $C_2(r)$ at the stationary state can be determined exactly and used to test the previous dimensional arguments. In the shear-free case, $\sigma = 0$, the problem is isotropic and the expression for $C_2(r)$ is well-known analytically. The inertial-range scaling behaviour for the second-order structure function $S_2(r) = \{\chi(0)/[2 - \xi)D]\} r^{2-\xi}$, where $\chi(0)$ is the scalar variance injection rate. The exponent $2 - \xi$ is in agreement with the Lagrangian dimensional estimate.
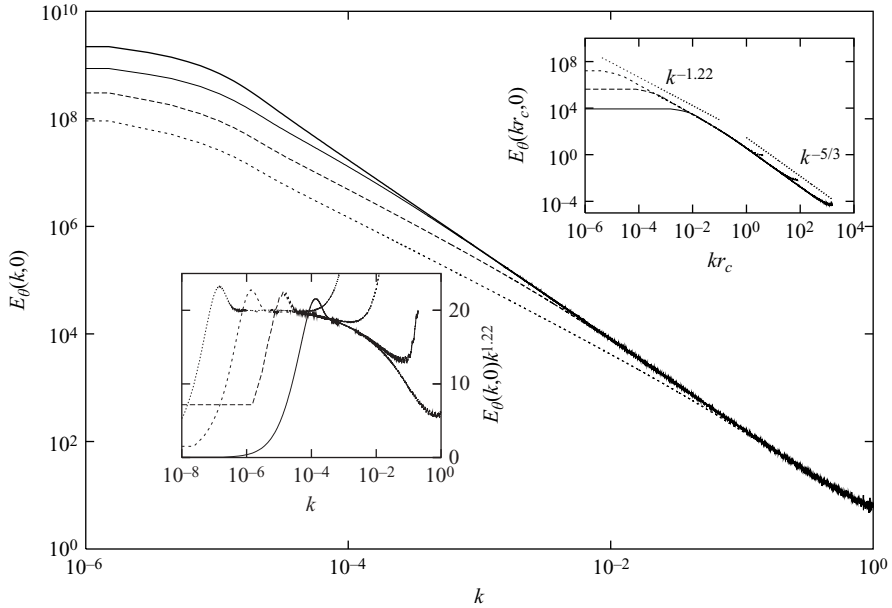
FIGURE 1. Scalar spectra in the x-direction, $E_\theta(k,0)$, obtained by fixing $D = 0.05$ and varying σ (from top to bottom, $\sigma = 0, 0.0004, 0.0036, 0.025$). In the numerical computations L_{box} and L_f have been fixed to 128^3 and 10^5, respectively – see the Appendix for the definition of the parameters – and the scaling exponent of the velocity $\xi = 4/3$. The inset at the top right shows the rescaled spectra $E_\theta(kr_c, 0)$ *vs.* kr_c. At large wavenumbers, the $k^{-5/3}$ spectrum is recovered, while at small k the power law $k^{-11/9}$, predicted by Lagrangian dimensional arguments, appears. The inset at the bottom left shows the compensated spectra $E_\theta(k,0)k^{11/9}$ obtained by fixing $\sigma = 0.025$ and varying $L_f = 10^4, 10^5, 10^6, 10^7$. The number of harmonics ℓ^*, the box size L_{box} and the number of grid points have been varied accordingly. Note that the transition region to the asymptotic slope $-11/9$ is quite broad.

In the presence of shear, the equation for the second-order correlation function is still closed, but the problem is not isotropic anymore. Following the same procedure as in the shear-free case (Kraichnan 1968), one obtains

$$\partial_t C_2 + \sigma(r\sin\phi\cos\phi\,\partial_r - \sin^2\phi\,\partial_\phi)C_2$$
$$= \frac{1}{r}\partial_r(Dr^{1+\xi} + 2\kappa r)\partial_r C_2 + \frac{1}{r^2}[(1+\xi)Dr^\xi + 2\kappa]\partial_\phi^2 C_2 + \chi(r), \quad (4.3)$$

where $\boldsymbol{r} = (r, \phi)$ denotes the relative distance between the two points. The forcing is taken to be Gaussian, statistically homogeneous and isotropic, with zero mean and correlation function $\langle f(\boldsymbol{r},t)f(0,0)\rangle = \delta(t)\chi(r)$. In the simulations, the correlation function of the forcing is taken as $\chi(r) = \exp(-r^2/2L_f^2)$. Contrary to the δ-correlation of the velocity, the previous hypotheses on the forcing are not restrictive and might be easily relaxed. The anisotropy induced by the shear means that C_2 will depend both on r and on the angle ϕ between $\boldsymbol{r}$ and the x-axis. The steady-state solution of (4.3) cannot be obtained analytically anymore and we have to resort to numerical methods (see the Appendix for details).

The existence of a crossover scale, r_c, separating the scales dominated by the turbulence and those affected by the shear, is easily recognized by a direct inspection of (4.3). A simple balance of the shear and the eddy-diffusivity terms in (4.3) gives $r_c \sim (D/\sigma)^{1/(2-\xi)}$. The crossover is evident in figure 1, where the scalar spectrum for
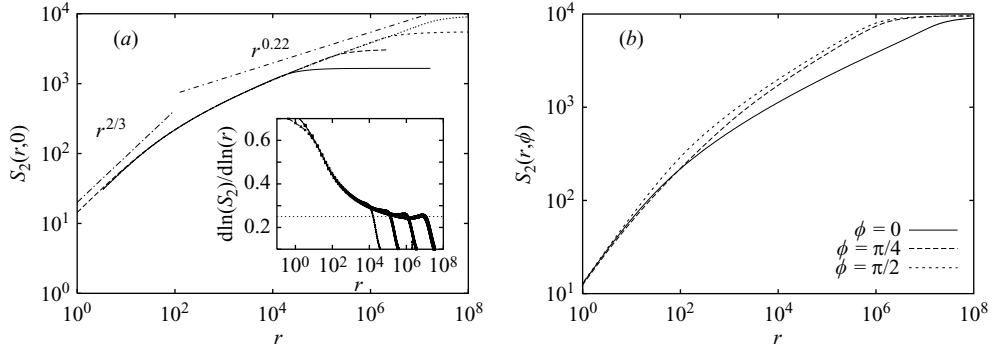
FIGURE 2. (a) The scalar second-order structure function measured in the x-direction, $S_2(r, 0)$, fixing σ and varying L_f (as in the bottom inset of figure 1). The inset shows the local slopes. Note that the approach to the asymptotic scaling $r^{0.22}$ is even slower than in the spectra. (b) The scalar second-order structure function measured at different angles, $S_2(r, \phi)$, for the case $\sigma = 0.025$ and $L_f = 10^7$. The statistics becomes more and more anisotropic as larger scales are considered. A similar behaviour is observed for the spectra (not shown).

$\xi = 4/3$ in a wide span of scales is reported. The results are in agreement with the Lagrangian predictions (4.2), with $E_\theta(k) \sim k^{-5/3}$, for $kr_c \gg 1$, and $E_\theta(k) \sim k^{-11/9}$ asymptotically reached at the large scales. Moreover, as shown in the top right inset, the spectra obtained with different shear rates all collapse by rescaling the wave-numbers kr_c.

The corresponding behaviour in physical space for the second-order structure function is shown in figure 2(a). Two regimes are again clearly visible. A point to be noted in the inset is that the convergence to the asymptotic slope, $S_2(r) \sim r^{2/3}$, is even slower than in k-space. The behaviour of the second-order structure function for different orientations is shown in figure 2(b). As expected in a range of scales affected by the shear, the anisotropy is strong and the crossover between the two previous regimes depends on the angle of measurement. It would be very informative to have similar measurements of the anisotropy in experimental conditions.

Note, as an aside, that an asymptotic expansion valid for small angles can be found analytically. Indeed, the correlation function C_2 can be expressed as

$$C_2(r_x, r_y) = (D/\sigma)^{-1/3} r_x^{(2-\xi)/3} f\left[r_y / \left(Dr_x^{1+\xi}/\sigma\right)^{1/3}\right], \qquad (4.4)$$

where the angular part f obeys the equation

$$f''(w) + \frac{w^2}{3} f'(w) - \frac{w}{(1+\xi)} f(w) = -\frac{\chi}{\sigma(1+\xi)}. \qquad (4.5)$$

For small angles, i.e. $w \ll 1$, the operator appearing in (4.3) reduces to $\sigma r_y \partial_{r_x} - D(1+\xi) r_x^\xi \partial_{r_y}^2$ and it is easy to check that the solution to (4.5) has the form (4.4) with the function f behaving as

$$f(w) = -1 - \frac{\chi w^2}{2\sigma(1+\xi)} - \frac{w^3}{6(1+\xi)} + O(w^4).$$

An even closer contact to the Lagrangian arguments (4.2) is made by directly simulating the equations of motion for the tracer particles. The method used for the simulations is the same as in Frisch, Mazzino & Vergassola (1998). Figure 3 presents the evolution of the particle separation for $\xi = 4/3$. As long as $\langle R^2(t) \rangle < r_c^2 \sim$
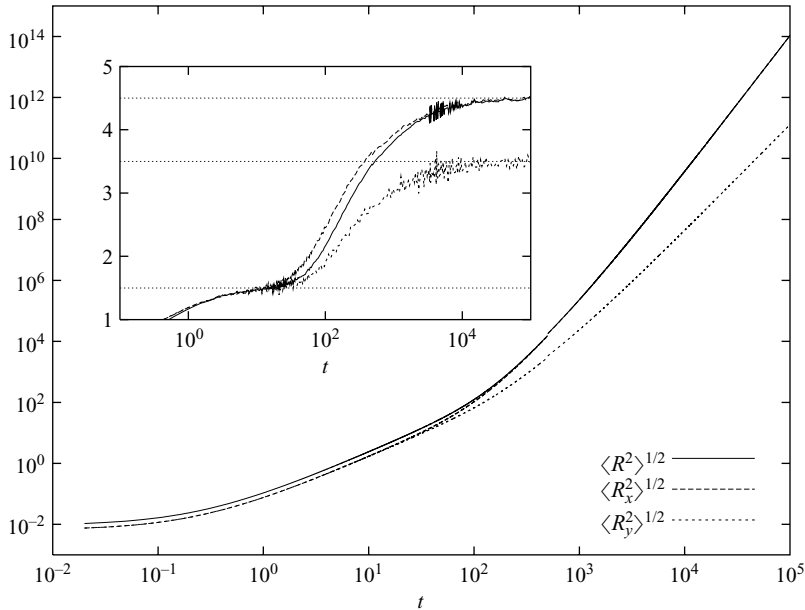
FIGURE 3. The curves of the Lagrangian separations as a function of time, for a Kraichnan flow with exponent $\xi = 4/3$. At small times, $\langle R_x^2(t) \rangle = \langle R_y^2(t) \rangle = \langle R^2(t) \rangle/2 \sim t^3$, as expected according to the Richardson law. At large times, $\langle R^2(t) \rangle \approx \langle R_x^2(t) \rangle \sim t^9$ and $\langle R_y^2(t) \rangle \sim t^7$, in agreement with (4.2). The inset displays the local slopes as a function of time. Note the wide crossover region between the two regimes. The numerical integrations of (3.5) and (3.6) have been performed following the point-splitting scheme described in Frisch *et al.* (1998), i.e. with molecular diffusivity $\kappa = 0$ and taking the initial separation small but finite.

$(D/\sigma)^{2/(2-\xi)}$, the Richardson prediction is recovered and the anisotropy induced by the shear is negligible. As the separation becomes larger compared to r_c, the trajectories are more affected by the shear and $\langle R^2 \rangle \approx \langle R_x^2 \rangle \gg \langle R_y^2 \rangle$. In this range of scales, $\langle R_x^2 \rangle$ and $\langle R_y^2 \rangle$ grow with two different power laws and the local slopes in the inset of figure 3 are found to be in agreement with (4.2). The predictions (4.2) and the numerical simulations are found to be in agreement for values of $\xi \neq 4/3$ as well (data not shown).

Note that the Lagrangian numerics shows a wide crossover region between the two different regimes (see figure 3). That is the reason for the very slow convergence of the scalar structure functions and spectra to their asymptotic slopes. In general, detecting the transition between the inertial–convective and the shear regimes demands a very broad range of accessible scales.

We finally consider the case where the shear is random. If its direction is fixed and the time scale of its intensity is short, the resulting exponent of the scalar spectrum is $-2 + \xi/2$. If both the direction and the intensity of the shear rapidly fluctuate in time, i.e. the shear is a Kraichnan flow with $\xi = 2$, isotropy is recovered and the scalar correlation function in the stationary state obeys $(1/r)\partial_r(\sigma r^3 + Dr^{1+\xi} + 2\kappa r)\partial_r C_2 = -\chi(r)$. The equation is easily solved analytically and the ensuing slopes of the scalar spectra are $-3 + \xi$ at small scales (large wavenumbers) and -1 at large scales (small wavenumbers).

5. Conclusions

The results presented here illustrate the presence of a new shear regime for a passive scalar transported in turbulent shearflows. The scale of crossover between the

classical Obukhov–Corrsin range and the larger scales, where the effects of the shear are felt, is proportional to the ratio between the turbulent and the shear intensities. The range of scales where the shear regime is observed then becomes parametrically large on increasing the shear rate. In experiments where the latter is fixed, increasing the turbulence intensity has the double effect of decreasing the Kolmogorov scale and increasing the crossover length r_c. The Obukhov–Corrsin scaling is therefore observed over a broader and broader range of scales. When r_c is much larger than the integral scale L of the scalar, the picture at scales $\leqslant L$ becomes essentially shear free. For $r_c \simeq L$, the presence of the shear range is still relevant due to the crossover effects which induce a scalar spectrum shallower than $-5/3$ and anisotropic. Those effects disappear quite slowly with the Reynolds number due to the broad span of scales required for the crossover. Furthermore, we have shown that the scalar spectrum in the shear region is sensitive to the geometry and the fluctuations of the shear. Experiments with different set-ups, where the shear components have drastically differing properties, might then yield different scalings at asymptotically large scales. All are shallower than $-5/3$, though, and therefore inducing crossover effects that tend to flatten out the scalar spectrum. In those conditions where shear fluctuations in intensity and direction are controlled, we specifically predict the existence of a $k^{-4/3}$ asymptotic regime. This picture seems to account for the major points in the experimental observations presented in §2.

Two issues for future investigation are the following. Theoretically, it is quite likely that the shear will affect the scalar higher-order statistics; the resulting behaviours remain to be clarified. Experimentally, it would be of interest to have a set-up where the Reynolds number is kept fixed and the shear rate is increased, in well-controlled conditions, so as to enlarge the shear regime and quantitatively analyse its properties.

Appendix. Equations for the correlation function and numerical computation

The anisotropy introduced by the shear can be handled by using polar coordinates, which allow the correlation function to be decomposed as:

$$C_2(\boldsymbol{r}, t) = C_2(r, \phi, t) = F_0(r, t) + \sum_{\ell=1}^{\infty} F_\ell(r, t) \cos(2\ell\phi) + \sum_{\ell=1}^{\infty} G_\ell(r, t) \sin(2\ell\phi). \quad \text{(A 1)}$$

Here, ℓ labels the order of the harmonics. Note that only even harmonics are present for symmetry reasons. Substituting (A 1) into (4.3), one obtains the following set of 1+1 dimensional partial differential equations:

$$\partial_t F_\ell + \sigma \frac{r}{4}[\partial_r G_{\ell+1} - \partial_r G_{\ell-1}] + \frac{\sigma}{2}[(\ell+1)G_{\ell+1} - 2\ell G_\ell + (\ell-1)G_{\ell-1}]$$
$$= \frac{1}{r}\partial_r[2\kappa r + Dr^{1+\xi}]\partial_r F_\ell - [2\kappa + (1+\xi)Dr^\xi]\frac{4\ell^2}{r^2}F_\ell + \delta_{\ell,0}\chi, \quad \text{(A 2)}$$

$$\partial_t G_\ell - \sigma \frac{r}{4}[\partial_r F_{\ell+1} - (1+\delta_{\ell,1})\partial_r F_{\ell-1}] - \frac{\sigma}{2}[(\ell+1)F_{\ell+1} - 2\ell F_\ell + (\ell-1)F_{\ell-1}]$$
$$= \frac{1}{r}\partial_r[2\kappa r + Dr^{1+\xi}]\partial_r G_\ell - [2\kappa + (1+\xi)Dr^\xi]\frac{4\ell^2}{r^2}G_\ell. \quad \text{(A 3)}$$

Note that the coupling among the harmonics is indeed due to the shear term.

These equations have been numerically integrated for times long enough to reach a stationary state. The correlation function $C_2(r, \phi)$ is then computed at different orientations ϕ from $F_\ell(r)$ and $G_\ell(r)$ by using (A 1). The second-order structure function $S_2(r, \phi) = 2(C_2(0) - C_2(r, \phi))$ easily follows, as does the scalar spectrum $E_\theta(k, \phi)$, which is obtained by a one-dimensional Fourier transform.

The equations have been solved for various choices of the parameters. In practice, we have fixed D and varied σ and L_f. For the boundary conditions at the origin, we have taken $F_0'(0) = 0$, $G_\ell(0) = 0$ for each ℓ and $F_\ell(0) = 0$ for $\ell > 0$. The infrared boundary condition has been fixed by setting to zero the values of all the functions $F_\ell(r)$ and $G_\ell(r)$ beyond $r = L_{box}$. The maximum size of the system, L_{box}, has been taken much larger than the forcing scale L_f to properly resolve the anisotropic contributions.

REFERENCES

BATCHELOR, G. K. 1959 Small-scale variation of convected quantities like temperature in turbulent fluid. Part 1. General discussion and the case of small conductivity. *J. Fluid Mech.* **5**, 113–133.

CASCIOLA, C. M., BENZI, R., GUALTIERI, P., JACOB, B. & PIVA, R. 2002 Double scaling and intermittency in shear dominated flows. *Phys. Rev.* E **65**, 015301.

CORRSIN, S. 1951 On the spectrum of isotropic temperature field in isotropic turbulence. *J. Appl. Phys.* **22**, 469–473.

FALKOVICH, G., GAWĘDZKI, K. & VERGASSOLA, M. 2001 Particles and fields in fluid turbulence. *Rev. Mod. Phys.* **73**, 913–975.

FRISCH, U., MAZZINO, A. & VERGASSOLA, M. 1998 Intermittency in passive scalar advection. *Phys. Rev. Lett.* **80**, 5532–5535.

JAYESH, TONG, C. & WARHAFT, Z. 1994 On temperature spectra in grid turbulence. *Phys. Fluids* **6**, 306–312.

KRAICHNAN, R. H. 1968 Small-scale structure of a scalar field convected by turbulence. *Phys. Fluids* **11**, 945–963.

LEVÈQUE, M. A. 1928 Les lois de la transmission de la chaleur par convection. *Ann. Mines* **13**, 201–239.

MESTAYER, P. 1982 Local isotropy and anisotropy in a high-Reynolds number turbulent boundary layer. *J. Fluid Mech.* **125**, 475–503.

MILLER, P. L. & DIMOTAKIS, P. E. 1996 Measurement of scalar power spectra in high Schmidt number turbulent jets. *J. Fluid Mech.* **308**, 129–146.

MYDLARSKI, L. & WARHAFT, Z. 1998 Passive scalar statistics in high-Péclet-number grid turbulence. *J. Fluid Mech.* **358**, 135–175.

OBUKHOV, A. M. 1949 The structure of the temperature field in a turbulent flow. *Izv. Akad. Nauk. SSSR, Ser. Geogr. Geophys.* **13**, 58–69.

SIGGIA, E. D. 1994 High Rayleigh number convection. *Annu. Rev. Fluid Mech.* **26**, 137–168.

SREENIVASAN, K. R. 1991 On local isotropy of passive scalars in turbulent shear flows. *Proc. R. Soc. Lond.* A **434**, 165–182.

SREENIVASAN, K. R. 1996 The passive scalar spectrum and the Obukhov-Corrsin constant. *Phys. Fluids* **8**, 189–196.

STAICU, A. & VAN DE WATER, W. 2003 Small-scale velocity jumps in shear turbulence. *Phys. Rev. Lett.* **90**, 094501–094505.

VILLERMAUX, E., INNOCENTI, C. & DUPLAT, J. 2001 Short circuits in the Corrsin-Obukhov cascade. *Phys. Fluids* **13**, 284–289.

WARHAFT, Z. 2000 Passive scalars in turbulent flows. *Annu. Rev. Fluid Mech.* **32**, 203–240.

YEUNG, P. K., XU, S. & SREENIVASAN, K. R. 2002 Schmidt number effects on turbulent transport with uniform mean scalar gradient *Phys. Fluids* **14**, 4178–4191.